Supplementary Information for Quantitative absorption spectroscopy of few perovskite nanocrystals using cavity-enhanced imaging

Ines Amersdorffer[1,2,†], Andreas Singldinger[3,†], Nina A. Henke[3], Anna Abfalterer[3], Patrick Ganswindt[3], Jonathan Noé[1,*], Thomas Hümmer[1,*], David Hunger[2], Alexander S. Urban[3,*]

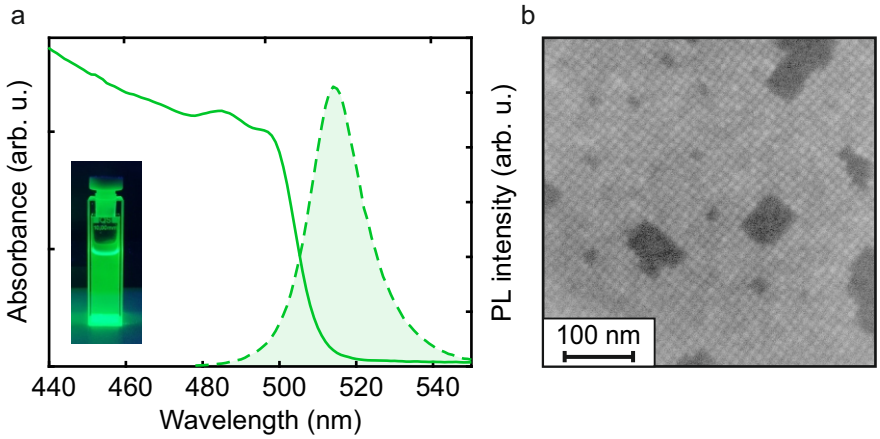

Figure S1: Optical and structural characterization of $CsPbBr_3$ nanocubes (**a**) Steady-state absorption spectrum (solid line) and PL spectrum (dashed line) showing a sharp absorption onset and a PL emission peak near 514 nm, typical of 8–9 nm large $CsPbBr_3$ nanocubes. The inset shows a photograph of $CsPbBr_3$ nanocubes in a cuvette under UV light illumination. (**b**) Representative SEM image of a $CsPbBr_3$ nanocube thin film confirming uniform cubic morphology and a mean nanocube edge length of (8.7 ± 1.0) nm. These measurements verify the size, shape, and optical quality of the nanocubes.

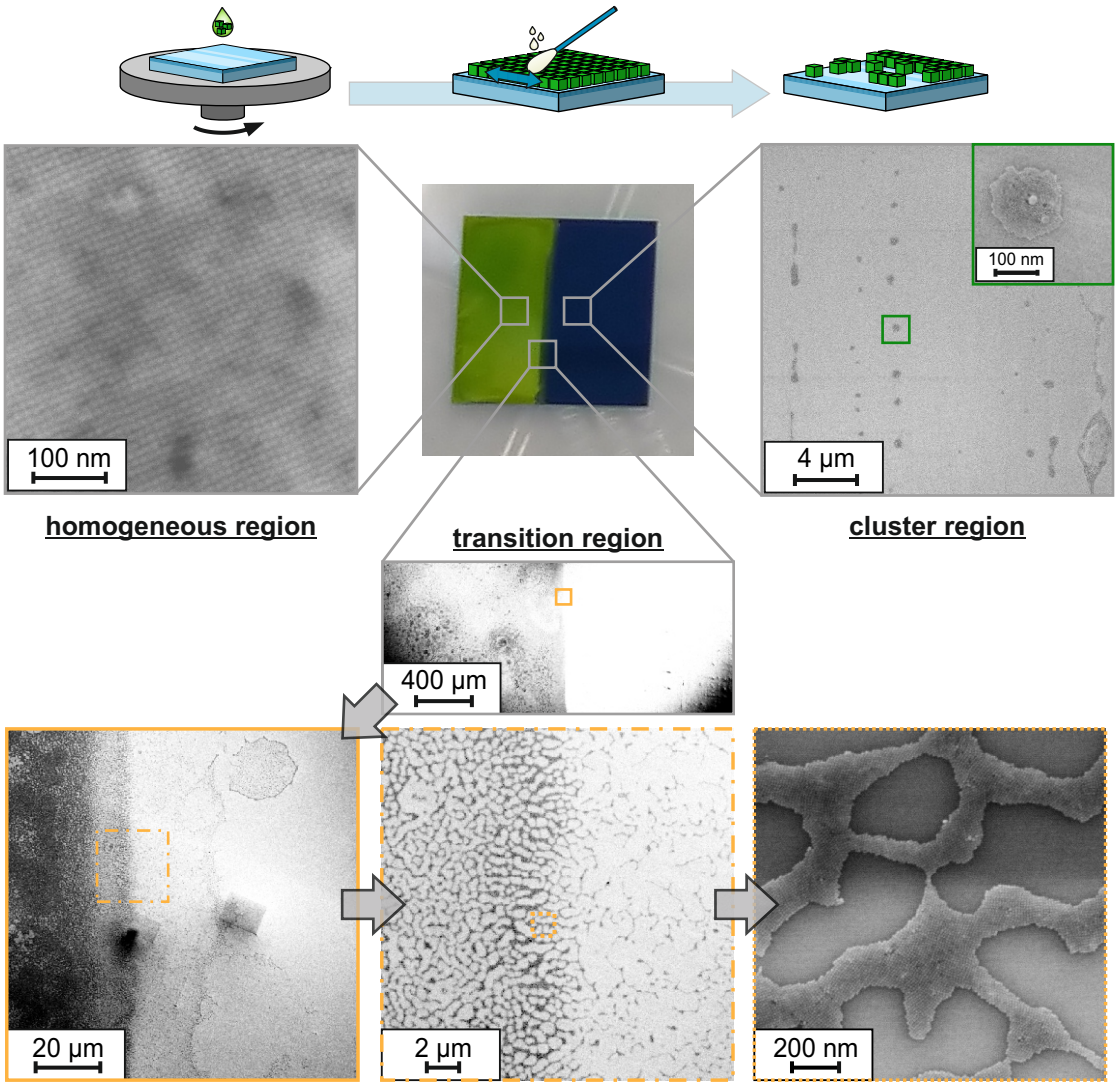

Figure S2: Preparation regions after selective wiping of thin films. Photograph and schematic illustrate three characteristic zones: a dense film, a transition area, and a sparse cluster region. SEM imaging on a Si substrate confirms reproducible generation of isolated nanocrystal clusters in the wiped region, suitable for high-sensitivity iCEAS measurements.

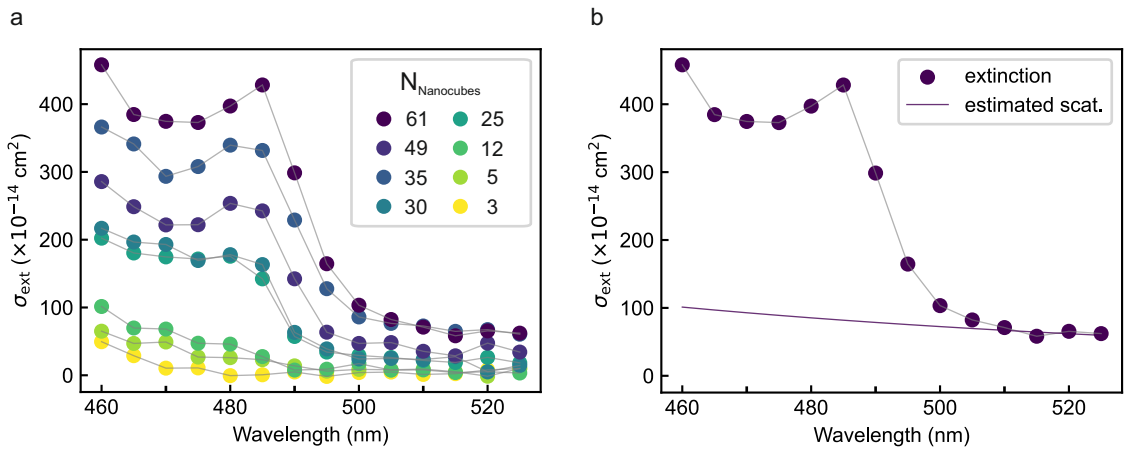

Figure S3: Spectral extinction and estimated contribution by scattering. (**a**) Raw extinction spectra for the differently sized nanocube clusters. (**b**) Extinction spectrum (solid line) with fitted Rayleigh-type scattering contribution, used to derive the corrected absorption spectra presented in the main text (Fig. 4c). Shown here for the cluster consisting of 61 nanocubes as an example.

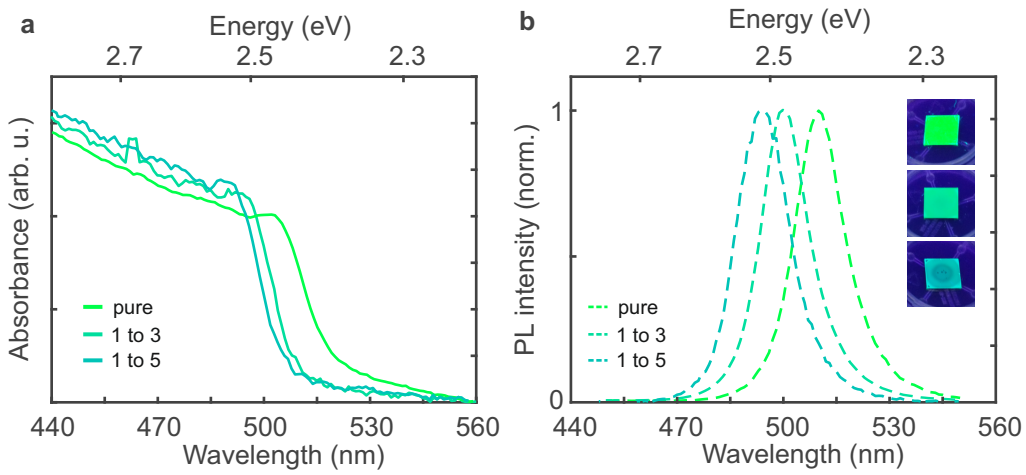

Figure S4: Effect of dispersion dilution on optical properties of $CsPbBr_3$ films. (**a**) Absorption spectra for pure and diluted (1:3 and 1:5, v/v in solvent) $CsPbBr_3$ nanocube dispersions prepared as thin films . A progressive blueshift of the absorption onset with increasing dilution can be observed. (**b**) Corresponding PL spectra of thin film samples exhibit the same blueshift, consistent with ligand loss and slight size reduction during film formation from more dilute solutions. The inset shows photographs of the corresponding thin films under UV light illumination.

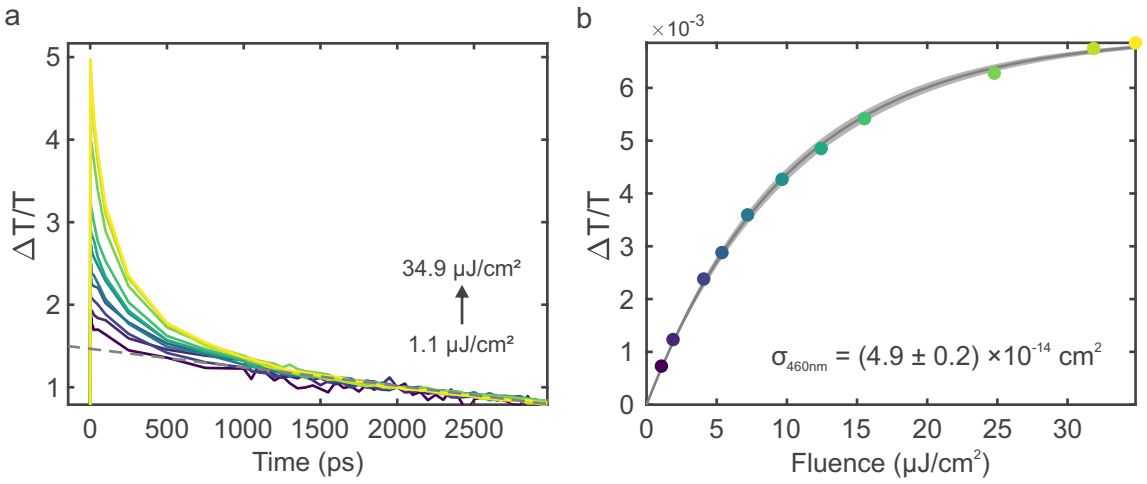

Figure S5: Transient-absorption benchmark for determining σ_{abs}. (**a**) Time-dependent photobleach signals ($\lambda_{bleach} = 506\,nm$) of $CsPbBr_3$ nanocubes in dispersion recorded at various excitation fluences, normalized at 2000 ps. (**b**) Linear dependence of late-time (2000 ps) photobleach intensity on excitation fluence yields a one-photon absorption cross-section of $\sigma_{460\,\mathrm{nm}} = (4.9 \pm 0.2) \times 10^{-14}\,\mathrm{cm}^2$. The strong agreement with iCEAS results validates the quantitative accuracy of the cavity-enhanced approach.

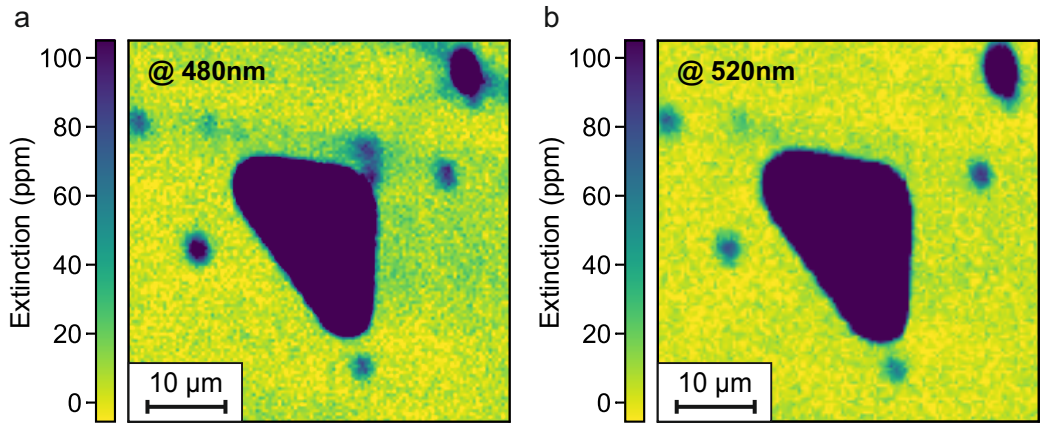

Figure S6: iCEAS extinction maps at different wavelengths. (**a**) Extinction image at 480 nm showing localized absorption from individual nanocube clusters. (**b**) Extinction image at 520 nm displaying reduced contrast and wavelength-dependent signal changes. Such hyperspectral maps allow reconstruction of absorption spectra for each cluster with sub-nanometer resolution.

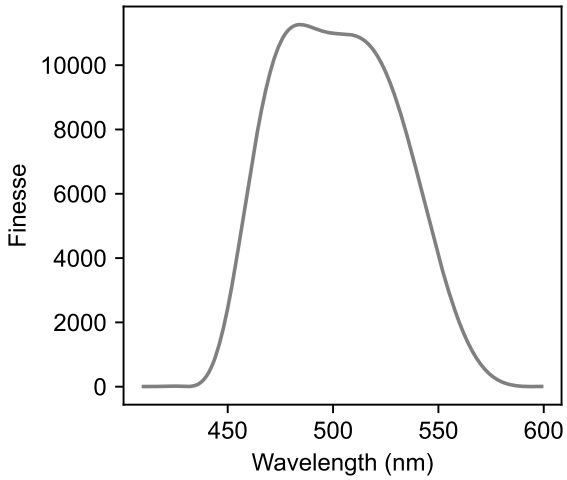

Figure S7: Simulated finesse of the optical cavity used in iCEAS measurements. The simulated finesse as a function of wavelength taking into account mirror performance above 99.95 % reflectivity in the 465–525 nm range and additional losses to match measured finesse values. The high level of finesse enables parts-per-million absorption sensitivity.

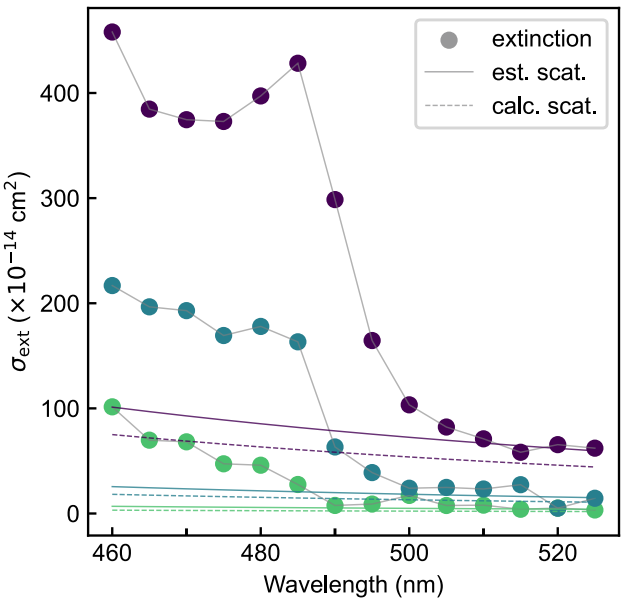

Figure S8: Comparison of estimated scattering contributions from experimental data and theoretical calculations using the polarizability tensor. The spectral extinction is shown with scatter points representing the experimental data, while the scattering contribution is estimated both from the measured data (solid line) and calculated using the polarizability tensor (dashed line). Results are presented for clusters of 12 (green), 30 (blue), and 61 (purple) nanocubes.

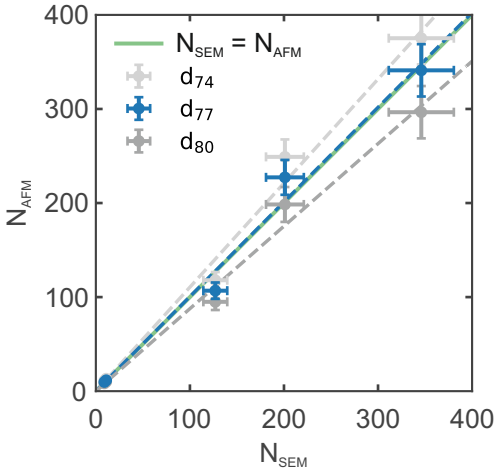

Figure S9: Comparison of AFM- and SEM-derived nanocube counts. The data points for using the 74th, 77th and 80th percentile of the height profiles and the corresponding linear fits (dashed lines) through them reveal that for the 77th percentile, the number of nanocubes counted in AFM agree best to the number counted in SEM.